Nanoscale

PAPER

View Article Online
View Journal | View Issue

Cite this: *Nanoscale*, 2026, **18**, 3669

Endovascular administration and magnetic retention of nanocapsules for improved brain delivery in large cerebral vascular models

Alba Grayston,[a] Miguel Garcia-Gabilondo,[a] Neus Otero-Fornés,[a] Anna Solé-Porta,[b] Itsasne de la Torre-Sánchez,[a] Wid Mekseriwattana,[b] Milan Timko,[c] Jozef Kovac,[c] Peter Kopcansky,[c] Jiahui Li,[d] Riccardo Tiberi,[d] Marielle Esteves,[e] Alejandro Tomasello,[d] David Hernández,[d] Marc Ribó,[d] Anna Roig[b] and Anna Rosell*[a]

Brain delivery remains a challenge for the clinical translation of therapeutic nanomedicines, particularly in focal diseases with specific delivery needs, such as stroke. In this scenario, clinically relevant endovascular interventions are recently being proposed as strategies to enhance delivery into specific cerebral vascular territories. In this study, we assess the feasibility of endovascular delivery and magnetic retention of biocompatible magnetic nanocapsules (NCs) in cerebral circulation models that better predict human responses. More specifically, polymeric NCs synthesized with magnetic properties (superparamagnetic oxide nanoparticles, SPIONs) and fluorescent (Cy5) moieties were infused into pigs *via* a femoral microcatheter reaching the brain vasculature and showing greater efficacy in targeting the ipsilateral brain hemisphere with preferential accumulation in microvessels when compared to intravenous administration which resulted in very little accumulation. Transient adverse effects related to hemodynamic instability upon nanocapsule administration were observed in both administration groups related to acute complement activation. Successful endovascular brain NC delivery is further demonstrated in a 3D-vascular model of the human large arterial vessel brain supply, with successful NC accumulation in the target arterial segment (the proximal middle cerebral artery) with sensible enhancement when using local magnetic fields. This study demonstrates the feasibility of endovascular NC delivery for focal brain nanotargeting *via* clinically relevant and minimally invasive procedures and proves the advantages of using magnetized nanomaterials to improve local vascular NC retention. Further safety and efficacy studies, including drug nanocapsule formulations, are needed to establish the clinical relevance of the proposed approach.

Received 12th August 2025,
Accepted 27th November 2025

DOI: 10.1039/d5nr03429a

rsc.li/nanoscale

Introduction

The use of nanomaterials in diagnosis and therapy is a rapidly evolving field that is advancing personalized treatments. Biocompatible polymeric nanocarriers offer significant advantages for delivering insoluble, sensitive, and multi-component drugs by protecting the therapeutic molecules.[1] However, efficient administration into injured tissues remains a significant challenge for nanomedicine as well as for many drug and cell therapies, with particular difficulties in achieving effective brain delivery. This limitation has hindered the development of neuroprotection and neurorepair-based strategies which, in the context of stroke disease, are essential beyond acute stroke recanalization management.[2]

Recent endovascular interventions utilizing microcatheters to navigate the arterial system and remove cerebral blood clots (mechanical thrombectomy) using stent retrievers or aspiration devices have provided an opportunity for direct therapeutic agent delivery into intracerebral vessels *via* a minimally invasive procedure.[3] The increasing use of these interventions in developed countries has opened new avenues for intra-arterial treatment delivery in specific vascular territories, as tested in stroke clinical trials with drug formulations and cell therapies[4,5] and previously proposed for drug delivery in brain

[a]*Neurovascular Research Laboratory, Vall d'Hebron Institut de Recerca, Universitat Autònoma de Barcelona (VHIR-UAB), 119-129 Barcelona, Spain. E-mail: anna.rosell@vhir.org*
[b]*Nanoparticles and Nanocomposites Group, Institut de Ciència de Materials de Barcelona (ICMAB-CSIC), Bellaterra, Spain*
[c]*Department of Magnetism, Institute of Experimental Physics, SAS, Kosice, Slovakia*
[d]*Stroke Unit & Stroke Research Group, Vall d'Hebron University Hospital-VHIR, Barcelona, Spain*
[e]*Experimental Surgery Unit-VHIR, Spain*

tumors[6] or during aneurysm coiling to treat thrombotic complications.[7] These approaches could be further adapted to enhance the delivery of various drug nanoformulations, incorporating multiple imaging and functional moieties, biocompatibility, biodegradability, and sustained-release properties.[8,9]

We have recently demonstrated that intra-arterial administration of magnetized nanocapsules (NCs) made of poly(D,L-lactic-*co*-glycolic acid) (PLGA), an FDA-approved polymer, combined with magnetic retention, can safely enhance brain NC delivery in the ipsilateral ischemic hemisphere in a mouse stroke model, overcoming the poor brain delivery observed with conventional intravenous administration.[10]

In the present study, we aimed to further translate this clinically relevant endovascular approach to a large animal model in pigs targeting larger cerebral vessels that offers several advantages for neurointerventional research. This includes features closely resembling human conditions, such as a gyrencephalic brain, a comparable gray-to-white matter ratio, similar arterial calibers, and analogous vascular brain territories, making the model well-suited for studies on safety, feasibility, and efficacy.[11] We complemented this approach by employing a unique 3D-printed model of the human large arterial vessel brain supply to test the intracranial microcatheter delivery in combination with a magnet device scaled for human application, aiming to evaluate the hypothesis that focused magnetic fields improve target NC retention in specific vascular areas.

Experimental section

Nanocapsule synthesis

All NC batches (hydrodynamic diameter 259 ± 31 nm) were synthesized using double emulsion solvent evaporation and surface functionalization with superparamagnetic iron oxide nanoparticles (SPIONs) for magnetic retention and Cy5 for fluorescence imaging, following previously described methods by our group[9] (for details, see the SI). Physicochemical stability and magnetic and imaging characteristics of the NCs have been thoroughly described in previous studies, showing synthesis robustness and reproducibility.[9,10,12,13] NC characterization related to the batches used in the present study is shown in Fig. 1A–D with additional details in the SI. A total of 22 independently synthesized batches were used in this study.

Nanocapsule delivery in pigs

Hybrid female pigs (large white × landrace, 33 to 40 kg; 3 months old) were purchased from A. M. Animalia Bianya S. L. (Girona, Spain) and reused from an interventional training course, adhering to the 3Rs principles in animal experimentation. All procedures were approved by the VHIR Ethics Committee for Animal Experimentation (29/22CEEA and approval no. 10257) in compliance with the Spanish and EU directives (2010/63/EU). Detailed information on animal housing and welfare is provided in the SI.

All animals were maintained under general anesthesia throughout the entire intervention. Initially, anesthesia was induced *via* intramuscular administration of a combination of ketamine (20 mg kg^{-1}), midazolam (0.5 mg kg^{-1}), and medetomidine (0.02 mg kg^{-1}). Next, an intravenous catheter was placed, and if necessary, propofol was administered to complete the induction. After preoxygenation, endotracheal intubation was performed, and all animals were connected to an anesthesia machine and mechanically ventilated. Anesthesia was subsequently maintained with sevoflurane (FeSev 1.9–2.5%), delivered in a mixture of air and oxygen (50 : 50). All animals received morphine for pain management, administered as an initial intramuscular bolus (0.5 mg kg^{-1}) followed by a continuous infusion (0.05 mg kg^{-1}) until the end of the procedure (euthanasia).

All animals were maintained under general anesthesia (sevoflurane 2.5%) for the entire intervention. For NC infusion, 80 mg (in 50 mL of saline) were administered intra-arterially or intravenously (n = 5 per group) at a rate of 1 mL min^{-1}. Intra-arterial procedures were conducted by experienced interventional neurologists or radiologists involving the cannulation of the right femoral artery using an 8Fr Brite Tip sheath introducer and navigating a microcatheter (Phenom 021, Medtronic, California) to the left or right ascending pharyngeal artery (ipsilateral side), proximal to the rete mirabile (Fig. 2A) with the support of fluoroscopy systems (either the OEC Elite from GE Healthcare or the CIO Spin 3D from Siemens). Intravenous administration was performed *via* marginal ear vein cannulation. After NC infusion, animals received 10 mL of saline to flush the catheter.

Blood samples were collected in serum-separating tubes from the jugular vein before, during (10, 20, and 30 min), and at the end of the infusion (60 min). Samples were centrifuged (1500*g*, 15 min, 4 °C), and the collected serum was stored at −20 °C for analysis. All animals were euthanized without recovery using intravenous sodium thiopental (2 g) at the end of the NC infusion when whole brains were removed and preserved in saline at 4 °C in the dark until *ex vivo* fluorescence molecular imaging (FMI) which was conducted within 24 h. Afterwards, brains were sliced in one cm sections and one square cm specimens were selected from those areas showing FMI signals in the ipsilateral hemisphere and corresponding contralateral areas (n = 3 per hemisphere). Those specimens were fixed with 4% PFA overnight and cryopreserved with 30% sucrose for 48–72 h before they were embedded in OCT. Finally, brain specimens were cryosectioned (12 μm sections) and stained as described below to assess Cy5-NC tissue distribution.

Fluorescence molecular imaging

FMI was conducted to characterize NC fluorescence *in vitro* (Fig. 1E and F) and track its distribution *ex vivo* in brain samples or within the 3D model using an IVIS® Lumina LT Series III imaging system (PerkinElmer). Full methodological details are available in the SI.

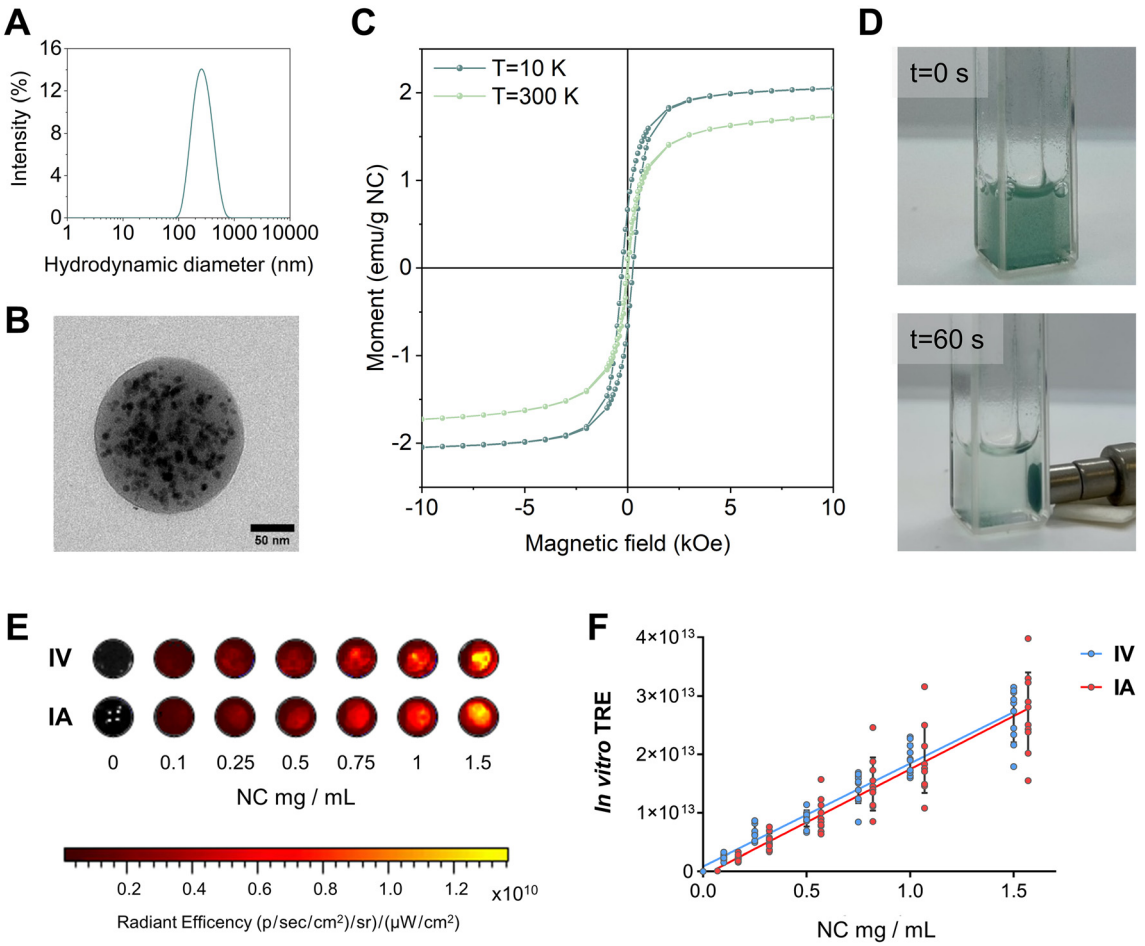

Fig. 1 Characterization of magnetic PLGA nanocapsules (NCs). (A) Intensity size distribution obtained by dynamic light scattering (DLS). (B) Transmission electron microscopy (TEM) image of a magnetic NC showing the homogeneous loading of SPIONs in the polymeric matrix. (C) Field-dependent magnetization curves of the magnetic NC measured at 10 K (dark green) and at 300 K (light green). The loading of SPIONs in the NC, estimated from the remanent magnetization, is approximately 10 wt%. (D) Magnetic retention of the NC at a concentration of 1.6 mg mL^{-1}. After 60 s, complete retention near the magnet is observed. The greenish coloration arises from the Cy5 dye incorporated into the NC. (E) Representative FMI images of increasing concentrations of Cy5 fluorescent NCs dispersed in saline *in vitro*. (F) Quantification of TRE on ROIs drawn for each plate well at increasing NC concentrations for batches used for intravenous (IV) or intra-arterial (IA) administration (n = 10 per group) in the study. Data are represented as mean ± SD.

For imaging quantification, regions of interest (ROIs) were manually drawn around the fluorescence signal, and total radiant efficiency (TRE; [photons per s]/[μW cm^{-2}]; Fig. 2) was measured using Living Image software (PerkinElmer, Waltham, MA). Fresh serum samples were used to measure circulating Cy5-NC fluorescence at various time points post-infusion. Briefly, 100 μL of each serum sample was plated in duplicate in 96-well plates, and fluorescence was measured using a microplate fluorescence reader ($\lambda_{ex}/\lambda_{em}$ 650/750 nm, respectively; Synergy Mx, BioTek Instruments Inc., USA). All post-infusion values were adjusted for baseline serum fluorescence of each sample.

Complement C3a serum determinations

Frozen samples were thawed to determine serum levels of complement fragment C3a which was measured using an enzyme-linked immunosorbent assay (ELISA) specific for pig C3a (Abbexa, Cat. No. Abx154897), following the manufacturer's instructions. Samples were diluted 1/1000 in PBS, analyzed in duplicate, and maintained within a coefficient of variation <20%.

Lectin-FITC vessel staining

Brain vasculature was stained to assess the distribution of Cy5-labeled NCs in 12 μm OCT-embedded brain sections (Fig. 3). Prior to staining, sections were fixed in 4% PFA and cryoprotected in 30% sucrose, embedded in OCT and frozen at −80 °C until analysis. Cryostat sections were thawed at 60 °C for 30 min, washed in PBS-1% Tween20 (PBS-T) for 3 min, and blocked with 3% BSA in PBS-T. Brain sections were then incubated for 1 h with FITC-labeled lectin from *Lycopersicon esculentum* (L0401, Sigma-Aldrich; 1 : 500 in 3% BSA PBS-T),

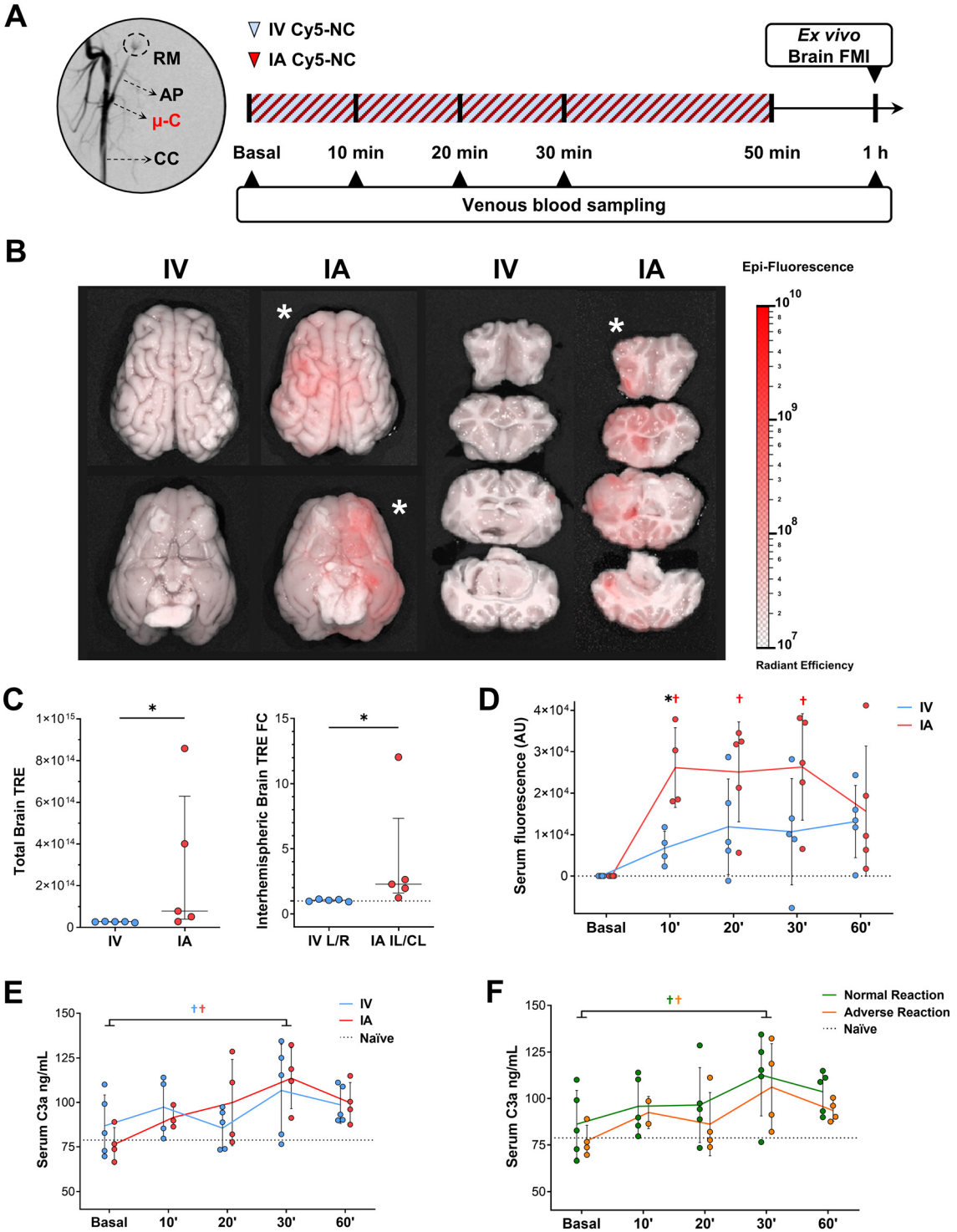

Fig. 2 Enhanced nanocapsule brain accumulation through endovascular delivery in pigs. (A) Experimental design and angiography image showing the micro-catheter (μ-C) position placed at the ascending pharyngeal (AP) artery proximal to the rete mirabile (RM). (B) Brain FMI images at 1 h after intra-arterial (IA)/intravenous (IV) NC administration in dorsal/ventral/coronal views. The white star indicates the hemisphere ipsilateral to the infusion site. (C) Bar graphs showing the Total Radiant Efficiency (TRE) quantification on total brain or interhemispheric fold change (FC) between the left (L) and right (R) hemispheres or ipsilateral (IL) and contralateral (CL) hemispheres in IV or IA (n = 5 per group), respectively; data are represented as median (IQR). (D) Time course of serum fluorescence (Arbitrary Units, AU) during infusion was corrected by the basal fluorescence; data are represented as mean ± SD (n = 5 per group). (E) Time course of the complement fragment C3a levels in serum obtained at different timepoints during NC infusion IV (n = 5) or IA (n = 4); data are represented as mean ± SD. (F) Serum C3a levels in individuals suffering an adverse reaction (n = 4) or not (n = 5) during NC administration; data represented as mean ± SD. In all graphs: *p < 0.05 between IV and IA, and †p < 0.01 *versus* the baseline.

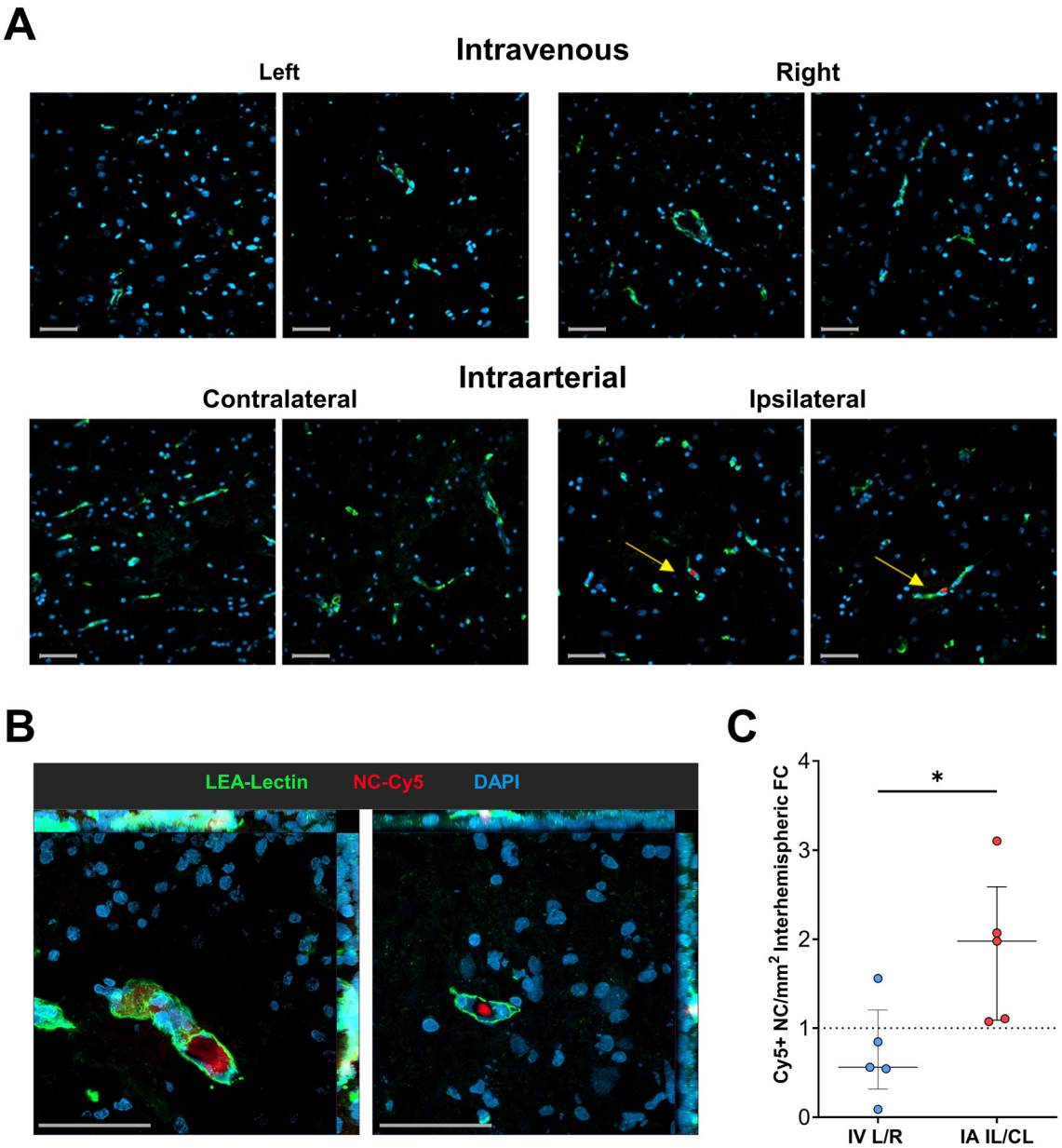

Fig. 3 Brain accumulation of nanocapsules after endovascular delivery. (A) Representative microscopy images of brain tissue immunofluorescence after intra-arterial (IA) and intravenous (IV) administration of Cy5-NC (red). Arrows show the Cy5-NC (red) in lectin-stained microvessels (green-stained). Cellular nuclei counterstained with DAPI (blue). (B) Representative images of *Z*-stack maximum intensity projection showing the Cy5 NC accumulation within microvessels in the IL hemisphere of IA animals. (C) Bar graph showing the Cy5 NC quantification per mm^2, represented as an interhemispheric fold change (FC), of the left (L) and right (R) hemispheres or ipsilateral (IL) and contralateral (CL) hemispheres in IV or IA, respectively. Data are represented as median (IQR). *$p < 0.05$. Scale bar represents 50 μm.

washed with PBS-T, and incubated for 15 min in 0.3% Sudan Black B (S2380, Sigma-Aldrich) to reduce autofluorescence. After additional washes with PBS-T, sections were mounted using VECTASHIELD® Antifade Mounting Medium with DAPI (H-1200, Vector Laboratories).

Widefield images were acquired using a Leica DMi8 Thunder Imager microscope at 10× magnification, and ImageJ software was used to quantify Cy5+ areas within selected ROIs, normalizing NC counts by area. Confocal images were obtained using a Zeiss LSM890 confocal microscope at 25× and 63× oil magnifications to localize Cy5+ signals within lectin-FITC+ microvessels.

Magnetic device design and characterization

A gold-coated FeNdB focused magnetic device prototype was designed adapted to the human anatomy, based on brain MRI images from anonymized subjects, as a wearable magnet for patients. The magnet was constructed using a patented

technology, GIAMAG© (GIAnt MAgnet field Gradient, Giamag Technologies, Norway), and was composed of multiple smaller segments to achieve maximum magnetic force. Segments of magnet are directed to a focal point 10 cm from the center of the magnet. The device consisted of a curved, focused magnet with a matrix of 16 partially gold-coated FeNdB magnet segments with a diameter of 40 mm and weight of 100 g (Fig. 4A and B).

The magnetic field and magnetic force were measured in the *X*–*Y*–*Z* axes according to the distance from the surface and the center of the magnet using a 3D Hall Probe (connected to a Gaussmeter GM-08). A semiautomatic *X*–*Y* scanner (Magscan) adapted with an Arduino microcontroller was used, and the *Z* axis was manually adjusted. Because the magnet is symmetrical, the magnetic field and the corresponding magnetic force (calculated from the magnetic field maps) were characterized for illustration purposes as a function of the distance from the center of the magnet and the distance above its surface, along the line where the individual segments are connected (*i.e.*, the gaps between segments).

Magnetic nanocapsule retention in a humanized model

The wearable magnet system was integrated into a 3D-printed model (described below) of the human supraaortic anatomy at the level of the middle cerebral artery (MCA) to evaluate its ability to retain infused NC within the MCA arterial segment (Fig. 4C). Additional manufacturing details can be found in the SI.

Computed tomography angiography (CTA) images of a 30-patient cohort who underwent mechanical thrombectomy were used to generate an anatomically representative 3D-printed vascular model to replicate anatomically relevant vessels for mechanical thrombectomy, including the common carotid arteries (CCAs), external carotid arteries (ECAs), internal carotid arteries (ICAs), MCAs, anterior cerebral arteries (ACAs), anterior communicating artery (ACoA), vertebral arteries (VAs), basilar artery (BA), posterior cerebral arteries (PCAs), and posterior communicating arteries (PCoAs), as shown in Fig. 4C. Patients with atherosclerotic disease were intentionally excluded when creating the cohort upon review of the CTA images. This selection ensured a standardized anatomical model with consistent vessel geometry and predictable flow dynamics, essential for the proof-of-concept evaluation of magnetic NC retention under controlled conditions. The model was printed with a commercially available photopolymer clear resin (Clear, FormLabs, Boston, MA, USA). Additionally, a 3D-printed temporal bone was fabricated using Durable Resin (FormLabs, Boston, MA). Further details on the 3D printing process are included in the SI.

For experimental testing, the magnet was attached to the 3D-printed temporal bone, targeting the MCA territory. A closed-circuit artificial bloodstream of water was generated using a peristaltic infusion pump, maintaining a constant inflow of 580 ml min^{-1}, which corresponds to 82% of the total cerebral blood flow (CBF) within the vascular model.[14] Carotid/vertebral distribution was 72%/28% of the total inflow (ICA = 210 mL min^{-1} per side, VA = 80 mL min^{-1} per side), and both target and ipsilateral MCA flow rate was approximately 150 mL min^{-1} (Fig. 4C). Control experiments were conducted under identical conditions without the use of the magnet.

In all experiments (n = 9), 20 mg of NCs (diluted in water at 10 mg mL^{-1}) were infused at a rate of 3 mL min^{-1} through an intermediate catheter (ACE 68, Penumbra), followed by a 4 mL water flush. The catheter was positioned at the level of the ICA and guided toward the MCA. NC deposition at the target site *versus* the contralateral side was evaluated using FMI after 1 h.

Statistical analysis

Statistical analyses were performed using GraphPad Prism 10 software. Normality of independent variables was assessed using the Shapiro–Wilk test (n < 30), and data were analyzed using either a t-test or a Mann–Whitney U test, as appropriate. For comparisons between brain hemispheres, a paired t-test was used, while time-course differences were assessed with a two-way ANOVA followed by Sidak's multiple comparisons test. For correlations, Spearman's test was applied. Data are presented as mean ± standard deviation (SD) for normally distributed variables or median and interquartile range (IQR) for non-normally distributed variables. Significance was set at p value <0.05, and statistical trend reported for values $0.05 \leq p < 0.1$.

Results and discussion

Magnetic nanocapsule characteristics

A comprehensive physicochemical, magnetic and fluorescence characterization of the magnetic PLGA-NC is presented in Fig. 1. The narrow intensity size distribution in Fig. 1A obtained by dynamic light scattering indicates the formation of uniformly sized NCs, with a mean hydrodynamic diameter of 259 ± 31 nm. The transmission electron microscopy (TEM) image in Fig. 1B reveals a spherical morphology of the nanocapsules and a homogeneous distribution of SPIONs attached to the surface. The field-dependent magnetization curves (Fig. 1C) demonstrate the magnetic character of the NC loaded with SPIONs. At 300 K, the absence of hysteresis indicates a superparamagnetic state, while at 10 K, the remanent magnetization (M_R), saturation magnetization (M_S), and coercivity (H_C) of the nanocapsules are 0.70 ± 0.04 emu g^{-1}, 2.2 ± 0.1 emu g^{-1}, and 264 ± 1 Oe, respectively. Comparison between the M_R values of SPIONs and NC gives an estimated SPIONs loading of approximately 10 wt%, which is similar to the values in previous studies.[9] In Fig. 1D, NCs at a concentration of 1.6 mg mL^{-1} are completely attracted to the magnet within 60 seconds, confirming their magnetic responsiveness. The greenish coloration of the suspension is due to the Cy5 dye incorporated into the nanocapsules. NC fluorescence was dose-dependent and consistent across all batches used in the different experiments of this study, as shown in Fig. 1E and F.

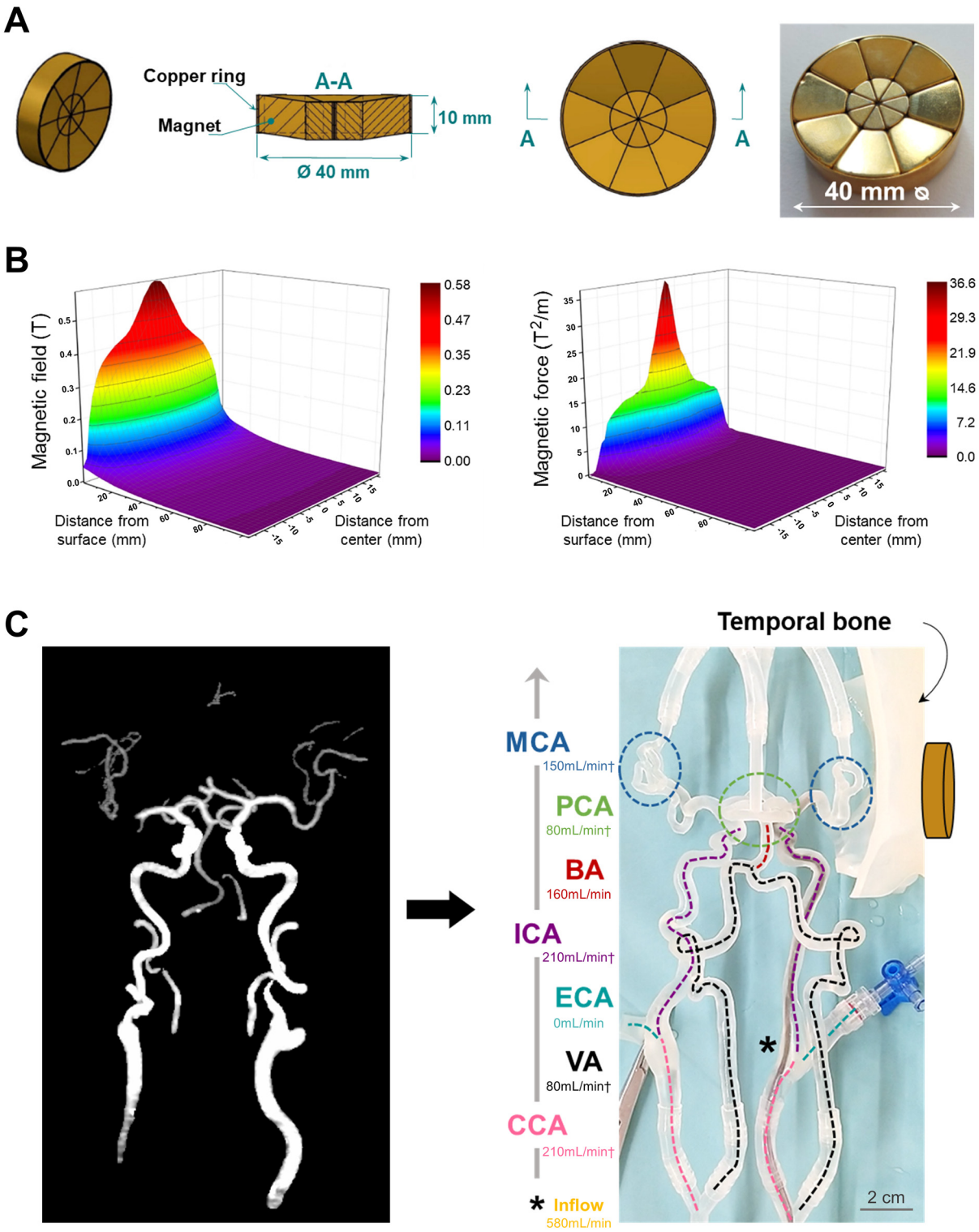

Fig. 4 Experimental set-up for endovascular NC delivery and magnetic retention in a humanized vascular model. (A) Scheme of the design and image of the focused magnet adapted to the human anatomy. (B) Graphs showing the magnetic field and magnetic force maps, measured by Magscan, at 10 mm above the magnet surface according to the distance from the surface and center of the magnet. (C) Representative CT angiography of a stroke patient following medical image processing (left) and a complete 3D-printed vascular model (right): the temporal bone and magnet position for catheter-facilitated (asterisk) NC infusion with magnetic targeting toward the MCA are shown. Blood flow distribution (mL min^{-1}) for each arterial segment is annotated following the same color code. PCA: posterior cerebral artery, BA: basilar artery, ECA: external carotid artery, VA: vertebral artery, MCA: middle cerebral artery, ICA: internal carotid artery, CCA: common carotid artery. †Blood flow rate per side, when applicable.

Endovascular administration improves NC delivery in the ipsilateral hemisphere in pigs

Biocompatible PLGA NCs have shown potential for enhancing brain drug delivery and improving therapeutic efficacy in various studies, highlighting the opportunities that nanomedicine offers for brain diseases such as stroke,[7,15,16] as well as the benefits of magnetic targeting in nanotechnology-assisted therapies.[17] In our previous study, we demonstrated the efficacy and safety of intra-arterially delivered magnetic biocompatible NC for focal brain therapy in stroke mice as well as its properties for *in vivo* brain tracking by both MRI and molecular imaging techniques due to its SPION and fluorescent surface moieties.[9,10] Here, we aimed to implement the system in large animals using clinically-relevant *in vivo* endovascular techniques for brain delivery, leveraging the potential advantages of magnetic targeting with a human-designed focused magnet device for external use in a 3D-printed model.

First, we show how the endovascular administration of NC in a clinically-relevant procedure was more effective in reaching the brain vasculature, as indicated by a significantly higher brain fluorescence signal compared to the intravenous route (7.86×10^{13} *vs.* 2.78×10^{13} TRE, $p = 0.01$), representing a 2.83-fold increase (Fig. 2B and C). Further analysis demonstrated that the intra-arterial route resulted in preferential NC accumulation in the desired (ipsilateral) hemisphere compared to the contralateral side. The interhemispheric fold-change difference was significantly higher in the intra-arterial route compared to the intravenous route (2.27 *vs.* 0.94, $p < 0.05$; Fig. 2C).

Cy5 NC fluorescence was detectable in serum during infusion in both groups. However, in the intra-arterial group, fluorescence was significantly higher at 10 min compared to the intravenous group (2.61×10^4 *vs.* 0.67×10^4 arbitrary units, $p < 0.01$), though not significantly different at 20 and 30 min ($p = 0.11$ and $p = 0.09$, respectively). Fluorescence levels equalized at the end of the infusion ($p = 0.76$). Additionally, serum fluorescence in the intra-arterial group was significantly higher than baseline at 10, 20, and 30 min ($p < 0.01$ for all time points; Fig. 2D), which was not significant in the intravenous group. This elevated fluorescence levels in serum collected from the brain circulation (jugular vein) following intra-arterial delivery further support improved brain delivery of the fluorescent NC within the first 30 min, although circulating bioavailability was short-lived.

In this regard, other NC have also been tested for intra-arterial administration in rodent models of cerebral ischemia, such as liposomal-encapsulated citicoline, which has demonstrated improved brain delivery,[18] or polymeric NC with resveratrol, which have exhibited neuroprotective and neurorepair effects,[19] among others. However, studies involving large animals with gyrencephalic brains and larger vascular structures (or humanized prototypes) remain scarce yet highly sought after in the translational pipeline. In this context, pigs have been widely used to develop humanized models and evaluate thrombectomy devices due to their cardiovascular similarities with humans,[20–22] making them suitable for this study despite anatomical differences such as the presence of the rete mirabile (a complex network of anastomosing vessels involved in cerebral blood hemodynamics) or the dual MCA per hemisphere. How these unique structures in the cerebral vascular anatomy could determine NC brain distribution or alter blood flow hemodynamics in the presence of circulating nanomaterials is unknown, but potential differences could be anticipated compared to human brain circulation.

Brain tissue localization of the nanocapsules

Brain tissue immunofluorescence confirmed focal NC accumulation in microvessels of the ipsilateral hemisphere compared to the contralateral areas (Fig. 3A and B), becoming significantly higher in animals that received intra-arterial infusion compared to those that received intravenous administration (1.98-fold *vs.* 0.56-fold change, $p = 0.03$), as shown in the NC quantification graph (Fig. 3C). These findings suggest a proper circulation and widespread brain distribution within the tissue of the target hemisphere after intra-arterial administration, although the mechanisms of accumulation at cellular/tissue level are not investigated. Previous investigations involving the use of PLGA-NC or other biocompatible polymers in rodents have already proved a rapid accumulation in off-target organs such as the liver, spleen, kidneys or lungs[9,10,23,24] with potential changes in organ distribution when applying endovascular targeting as proposed in our study. In this regard, our previous work in a mouse model of cerebral ischemia has reported larger accumulation of NC in the brain after intra-arterial administration accompanied by significant reductions of NC accumulation in abdominal organs such as the liver,[10] in line with other author investigations in a mouse model of hindlimb ischemia using larger magnetic microcapsules where the same delivery approach was used demonstrated a more efficient hind paw targeting than using the tail vein route, while reducing NC accumulation in abdominal organs as well.[24]

Although this is expected to also occur in both humans and large animals, further biodistribution and clearance studies are needed considering potential differences in capillary density, diameter of fenestrae, phagocytic behavior, or protein corona formation among species.

Tolerability of the nanocapsule administration in pigs

The interaction between nanoparticles and the immune system remains incompletely understood, and the administration of certain nanotechnology-based medicinal products has been associated with hypersensitivity reactions, primarily due to complement system activation (Complement Activation-Related Pseudoallergy, CARPA syndrome) to which pigs are particularly susceptible.[25,26] In this study, 4 out of 10 animals exhibited transient hyperacute adverse effects within the first 10 min of NC infusion, including a cutaneous rash and a sharp increase in cardiac frequency followed by a systemic hypotension (Fig. S1 in the SI). In three cases, this led to cardiac arrest, which was reversed with epinephrine adminis-

tration. NC infusion was continued in all animals and the measured physiological parameters progressively returned to normal values. NC-induced complement cascade activation was confirmed by measuring serum levels of the anaphylatoxin C3a fragment, which showed a significant increase at 30 min of infusion in both administration groups compared to baseline ($p < 0.01$; Fig. 2E). The increase in C3a levels was similar in animals with and without adverse reactions ($p < 0.01$; Fig. 2F) with no differences between groups at any time-point ($p > 0.05$). Additionally, the administered NC size was not different in those animals presenting adverse reactions and C3a serum levels were not related to either particle size nor Cy5+ NC fluorescence at any of the studied timepoints ($p > 0.05$, Fig. S2 in the SI). Strategies such as adjusting infusion rates have been reported to help prevent CARPA reactions,[27] as well as maintaining the particle size close to 200 nm since acute hemodynamic instability has been described for larger particle sizes following intravenous injection in pigs.[28] While such measures were implemented in this study, the appearance of CARPA syndrome is possible as confirmed by increased serum levels of the C3a anaphylatoxin during infusion in both administration groups, with several animals presenting severe hemodynamic instability, but not related to NC size nor to NC levels in circulation at the tested dose. Although a previous rodent study supported the safety of controlled intra-arterial PLGA NC administration at similar flow rates, this study was conducted in a species more sensitive to CARPA reactions[26] and in animals previously used for interventional training, which may have heightened their susceptibility. Importantly, these clinical manifestations were transient as reported by others,[22,28] and not related to the intra-arterial administration; however, this finding warrants further safety investigations such as the testing in other large animal species or the use of concomitant pharmacological interventions such as antihistamines, corticosteroids or fluid load, among others.[29]

Local nanocapsule targeting is feasible by combining endovascular delivery with magnetic retention

Additionally, we introduce a unique translational step by evaluating the potential use of an external magnet specifically designed for human application to retain NCs within specific arterial territories following endovascular administration, which could be used transiently during putative NC-based treatments. Previous studies in rodents have already tested the magnetic-delivery setup to guide/retain SPION-based nanoparticle treatments in stroke, glioma and cutaneous post-injury regeneration models.[10,30,31] In the present study, a focused magnet designed for NC retention in the 3D vascular model of the supraaortic circulation resembling the human anatomy generated a magnetic field of 0.6 T and a magnetic force close to 40 T^2 m^{-1} at 10 mm above the midline of the magnet along the main axis (Fig. 4A–C). FMI quantification analysis evaluating specific MCA targeting of intra-arterially infused NC (Fig. 5A–B) showed a significantly increased Cy5 signal in the targeted MCA at 1 h compared to the non-targeted contralateral MCA ($p = 0.03$ for control and $p = 0.01$ for magnetic targeting, Fig. 5C). Interhemispheric NC accumulation in the targeted MCA territory was greater in the model with magnetic retention with a strong statistical trend (2.96-fold *vs.* 1.47-fold, $p = 0.06$; Fig. 5C).

Using the same principles, a recent study also builds a proof of principle scalable magnetic device geometrically mimicking the surface of the head of a patient with a strength of 1.1 T and testing its retention capacity with a 3D-printed brain tumor phantom model with short exposure times,[30] as in our study. Our results align with the data obtained in the *in vivo* administration model in pigs, demonstrating preferential NC delivery to the MCA territory ipsilateral to the administration site and suggesting enhanced NC retention due to the magnetic field. The lack of statistical significance (despite a strong trend) may be related to the small sample size, the limited presence of smaller arterioles and capillaries in the 3D model, which restricts the retention capacity across the entire vascular network exposed to the magnetic fields, or the need for longer magnet-exposure times. Importantly, the potential bi-directional interaction between NC accumulation and blood flow in the 3D-model should be discussed. It has been reported that curved vessels and bifurcations create regions of disturbed flow, which may promote nanoparticle accumulation in off-target areas,[32] a phenomenon that could also occur in off-target regions of our model. Conversely, it is unlikely that NC accumulation in arterial segments would significantly narrow the vessel lumen or alter blood flow in our model, given the minimal narrowing observed in the assays (Fig. 5A) and prior studies indicating that changes in blood flow rate and velocity in MCA-M2 vessels occur only when luminal narrowing exceeds 60%.[33]

Limitations and future investigations

Our study paves the way for future studies where the therapeutic advantages of the proposed NC delivery approach should be evaluated using more complex 3D vascular models including smaller vessels, as well as in new pilot efficacy studies in stroke large animal models validated for neurointerventional procedures at short- and long-term.[11] These studies should be specifically designed to initially evaluate NC delivery efficiency relative to the total administered dose proving adequate delivery amounts and to ultimately test specific cerebroprotective or reparative treatments in brain disease models such as stroke, gliomas or traumatic brain injury, where focal delivery strategies could become a therapeutic advantage. In this regard, data from previous investigations using the proposed PLGA NC formulation in which albumin and VEGF were evaluated for protein encapsulation,[9,13] stablished the drug loading percentages at 1.1% and 0.5% respectively. Based on these previously reported values and considering the reached administration NC dose of 2.5 mg kg^{-1} of body weight in the present study, we could assume a potential drug delivery dose of 0.025 mg kg^{-1}, which is in the range of other tested compounds in preclinical studies in pigs (*e.g.*, 0.01 to 0.07 mg kg^{-1}).[34–37]

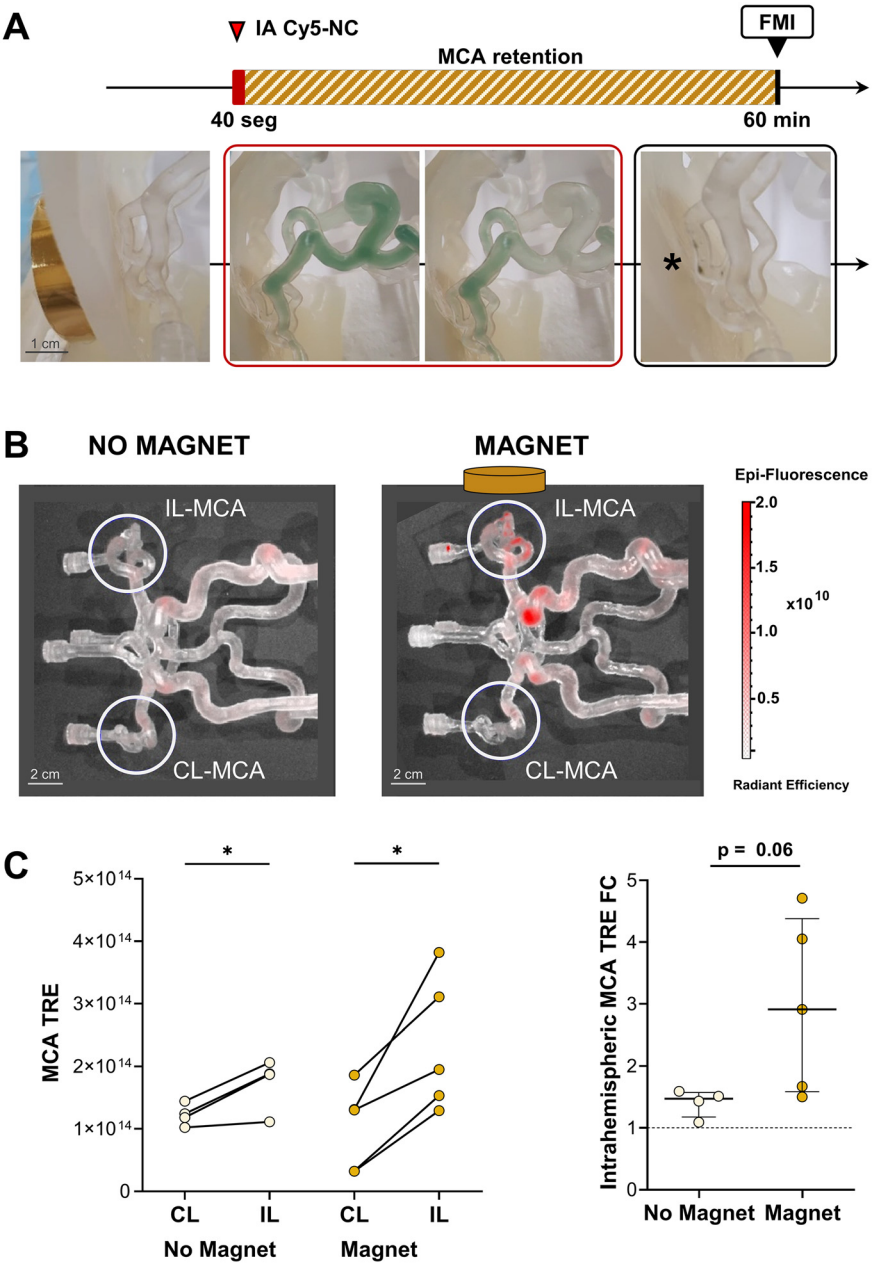

Fig. 5 Cy5-NC endovascular infusion and magnetic retention in a humanized 3D-model of the large arterial vessel brain supply. (A) Experimental design of the 3D model. Insets showing the MCA before, during and 1 h after infusion in a representative magnet retention experiment. The asterisk indicates NC deposition at the MCA under the magnet's influence at 60 min. (B) Representative FMI images and Total Radiant Efficiency (TRE) measure with or without magnet retention. Circles show the ROIs defined during quantification at the ipsilateral (IL) and contralateral (CL) MCA. (C) Graphs showing the TRE quantification at the MCA at the end of the experiment (1 h of perfusion) with or without magnet retention as raw data and as an interhemispheric fold change between the IL and CL MCA. Data are represented as median (IQR). *$p < 0.05$.

Conclusions

Nanomedicine holds great promise for treating brain diseases, including stroke, but faces significant challenges in bridging the gap between preclinical and clinical applications, particularly in achieving noninvasive, efficient brain delivery. Overall, our results demonstrate the successful endovascular administration of well-characterized monodisperse superparamagnetic and fluorescent PLGA NCs[9,12,13] using clinically relevant interventions to reach a specific brain hemisphere (ipsilateral to the administration site), showing a superior outcome to the traditional intravenous route, which resulted in poor brain NC accumulation. Additionally, the present study paves the way for the translation of brain nanotargeting *via* endovascular delivery and magnetic retention, offering a promising approach for multiple therapeutic agents.

Author contributions

A. G., M. G.-G., P. K., J. L., A. R. and A. R. designed and performed the experiments, collected and analyzed the data, and drafted the manuscript. N. O.-F., A. S.-P., I. T.-S., W. M., M. T., J. K., R. T., and M. E. performed the experiments and collected and analyzed the data. A. T., D. H. and M. R. conducted animal experiments. The authors revised and approved the manuscript.

Conflicts of interest

There are no conflicts to declare.

Data availability

The data supporting the findings and statistical results of this study are available in the supplementary information (SI). Supplementary information is available. Supplementary information includes: additional methods, Figure S1, Figure S2 and supplementary data supporting the experimental analysis. See DOI: https://doi.org/10.1039/d5nr03429a.

Additional raw data can be obtained upon reasonable request to the corresponding author.

Acknowledgements

The Euronanomed-MAGGBRIS project was supported by the Spanish Ministry of Science and Innovation (PCIN-2017-090), Instituto de Salud Carlos-III (AC17/00004 with FEDER funds) and Slovak Research and Development Agency (APVV-19-0324 and APVV-22-0060); 2021-SGR-0656 and 2021-SGR-00446 from AGAUR; SLT017/20/000197 from PERIS; RETICS from ISCIII (RD21/0006/0007 and RD24/0009/0020), the 'Severo Ochoa' Program (CEX2023-001263-S) and La Marató (202333-30). A.G was supported by an ISCIII fellowship (FI17/00073). A.S-P. is supported by a FPU fellowship (FPU21/04142) and is enrolled in the Materials Science Ph.D.-UAB. I.T-S is supported by a FI-STEP fellowship from AGAUR. We are grateful to Dr Yajie Zhang and to the VHIR Experimental Surgery Unit team.

When preparing this manuscript, the artificial intelligence tool ChatGPT (Open AI) has been utilized exclusively for refining English language expression and improving grammatical aspects. No data interpretation or discussion aspects have been generated using this or any other AI tool.

References

1 B. Begines, T. Ortiz, M. Pérez-Aranda, G. Martínez, M. Merinero, F. Argüelles-Arias and A. Alcudia, Polymeric Nanoparticles for Drug Delivery: Recent Developments and Future Prospects, *Nanomaterials*, 2020, **10**(7), 1403.

2 T. Bonnard, M. Gauberti, S. Martinez de Lizarrondo, F. Campos and D. Vivien, Recent Advances in Nanomedicine for Ischemic and Hemorrhagic Stroke, *Stroke*, 2019, **50**(5), 1318–1324.

3 J. Maingard, M. Foo, R. V. Chandra and T. M. Leslie-Mazwi, Endovascular Treatment of Acute Ischemic Stroke, *Curr. Treat. Options Cardiovasc. Med.*, 2019, **21**, 225–558.

4 V. H. E. Chen, G. K. H. Lee, C. H. Tan, A. S. T. Leow, Y. K. Tan, C. Goh, A. Gopinathan, C. Yang, B. P. L. Chan, V. K. Sharma, B. Y. Q. Tan and L. L. L. Yeo, Intra-Arterial Adjunctive Medications for Acute Ischemic Stroke During Mechanical Thrombectomy: A Meta-Analysis, *Stroke*, 2021, **52**(4), 1192–1202.

5 S. I. Savitz, D. Yavagal, G. Rappard, W. Likosky, N. Rutledge, C. Graffagnino, Y. Alderazi, J. A. Elder, P. R. Chen, R. F. Budzik Jr, R. Tarrel, D. Y. Huang and J. M. Hinson, Jr, A Phase 2 Randomized, Sham-Controlled Trial of Internal Carotid Artery Infusion of Autologous Bone Marrow-Derived ALD-401 Cells in Patients With Recent Stable Ischemic Stroke (RECOVER-Stroke), *Circulation*, 2019, **139**(2), 192–205.

6 R. Huang, J. Boltze and S. Li, Strategies for Improved Intra-arterial Treatments Targeting Brain Tumors: a Systematic Review, *Front. Oncol.*, 2020, **26**(10), 1443.

7 C. Mounayer, M. Piotin, S. Baldi, L. Spelle and J. Moret, Intraarterial administration of Abciximab for thromboembolic events occurring during aneurysm coil placement, *Am. J. Neuroradiol.*, 2003, **24**(10), 2039–2043.

8 J. Kong, R. Chu and Y. Wang, Neuroprotective Treatments for Ischemic Stroke: Opportunities for Nanotechnology, *Adv. Funct. Mater.*, 2022, **32**, 2209405.

9 Y. Zhang, M. García-Gabilondo, A. Grayston, I. V. J. Feiner, I. Anton-Sales, R. A. Loiola, J. Llop, P. Ramos-Cabrer, I. Barba, D. Garcia-Dorado, F. Gosselet, A. Rosell and A. Roig, PLGA protein nanocarriers with tailor-made fluorescence/MRI/PET imaging modalities, *Nanoscale*, 2020, **12**, 4988–5002.

10 A. Grayston, Y. Zhang, M. Garcia-Gabilondo, M. Arrúe, A. Martin, P. Kopcansky, M. Timko, J. Kovac, O. Strbak, L. Castellote, S. Belloli, R. M. Moresco, M. Picchio, A. Roig and A. Rosell, Endovascular administration of magnetized nanocarriers targeting brain delivery after stroke, *J. Cereb. Blood Flow Metab.*, 2022, **42**, 237–252.

11 A. M. Herrmann, S. Meckel, M. J. Gounis, L. Kringe, E. Motschall, C. Mülling and J. Boltze, Large animals in neurointerventional research: A systematic review on models, techniques and their application in endovascular procedures for stroke, aneurysms and vascular malformations, *J. Cereb. Blood Flow Metab.*, 2019, **39**(3), 375–394.

12 Y. Zhang, M. García-Gabilondo, A. Rosell and A. Roig, MRI/Photoluminescence Dual-Modal Imaging Magnetic PLGA Nanocapsules for Theranostics, *Pharmaceutics*, 2019, **12**(1), 16.

13 E. Carenza, O. Jordan, P. Martínez-San Segundo, R. Jiřík, Z. Starčuk Jr, G. Borchard, A. Rosell and A. Roig, Encapsulation of VEGF165 into magnetic PLGA nanocap-

sules for potential local delivery and bioactivity in human brain endothelial cells, *J. Mater. Chem. B*, 2015, **3**(12), 2538–2544.

14 L. Zarrinkoob, K. Ambarki, A. Wåhlin, R. Birgander, A. Eklund and J. Malm, Blood flow distribution in cerebral arteries, *J. Cereb. Blood Flow Metab.*, 2015, **35**, 648–654.

15 C. J. Love, M. Selim, M. Spector and E. H. Lo, Biomaterials for Stroke Therapy, *Stroke*, 2019, **50**, 2278–2284.

16 J. Ma, S. Zhang, J. Liu, F. Liu, F. Du, M. Li, A. T. Chen, Y. Bao, H. Won Suh, J. Avery, G. Deng, Y. Zhou, P. Wu, K. Sheth, H. Wang and J. Zhou, Targeted Drug Delivery to Stroke via Chemotactic Recruitment of Nanoparticles Coated with Membrane of Engineered Neural Stem Cells, *Small*, 2019, **15**, e1902011.

17 H. Liu, R. Sun, L. Wang, X. Chen, G. Li, Y. Cheng, G. Zhai, B. Bay, F. Yang, N. Gu, Y. Guo and H. Fan, Biocompatible Iron Oxide Nanoring-Labeled Mesenchymal Stem Cells: An Innovative Magnetothermal Approach for Cell Tracking and Targeted Stroke Therapy, *ACS Nano*, 2022, **16**, 18806–18821.

18 H. Liu, A. Jablonska, Y. Li, S. Cao, D. Liu, H. Chen, P. Cm Van Zijl, J. W. M. Bulte, M. Janowski, P. Walczak and G. Liu, Label-free CEST MRI Detection of Citicoline-Liposome Drug Delivery in Ischemic Stroke, *Theranostics*, 2016, **6**(10), 1588–1600.

19 X. Lu, J. Dong, D. Zheng, X. Li, D. Ding and H. Xu, Reperfusion combined with intraarterial administration of resveratrol-loaded nanoparticles improved cerebral ischemia-reperfusion injury in rats, *Nanomedicine*, 2020, **28**, 102208.

20 F. Arikan, T. Martínez-Valverde, A. Sánchez-Guerrero, M. Campos, M. Esteves, D. Gandara, R. Torné, L. Castro, A. Dalmau, J. Tibau and J. Sahuquillo, Malignant infarction of the middle cerebral artery in a porcine model. A pilot study, *PLoS One*, 2017, **12**, e0172637.

21 C. Castaño, M. Melià-Sorolla, A. García-Serran, N. DeGregorio-Rocasolano, M. R. García-Sort, M. Hernandez-Pérez, A. Valls-Carbó, O. Pino, J. Grífols, A. Iruela-Sánchez, A. Palomar-García, J. Puig, O. A. Martí-Sistac and T. Gasull, Establishment of a reproducible and minimally invasive ischemic stroke model in swine, *JCI Insight*, 2023, **8**(8), e163398.

22 D. T. Schomberg, A. Tellez, J. J. Meudt, D. A. Brady, K. N. Dillon, F. K. Arowolo, J. Wicks, S. D. Rousselle and D. Shanmuganayagam, Miniature Swine for Preclinical Modeling of Complexities of Human Disease for Translational Scientific Discovery and Accelerated Development of Therapies and Medical Devices, *Toxicol. Pathol.*, 2016, **44**, 299–314.

23 J. Sobska, B. Andreiuk, I. O. Aparin, A. Reisch, W. Krezel and A. S. Klymchenko, Counterion-insulated near-infrared dyes in biodegradable polymer nanoparticles for in vivo imaging, *Nanoscale Adv.*, 2021, **4**(1), 39–48.

24 O. A. Mayorova, O. A. Sindeeva, M. V. Lomova, O. I. Gusliakova, Y. V. Tarakanchikova, E. V. Tyutyaev, S. I. Pinyaev, O. A. Kulikov, S. V. German, N. A. Pyataev, D. A. Gorin and G. B. Sukhorukov, Endovascular addressing improves the effectiveness of magnetic targeting of drug carrier. Comparison with the conventional administration method, *Nanomedicine*, 2020, **28**, 102184.

25 Z. Wang and J. S. Brenner, The Nano-War Against Complement Proteins, *AAPS J.*, 2021, **23**(5), 105.

26 J. Szebeni, P. Bedőcs, D. Csukás, L. Rosivall, R. Bünger and R. Urbanics, A porcine model of complement-mediated infusion reactions to drug carrier nanosystems and other medicines, *Adv. Drug Delivery Rev.*, 2012, **64**(15), 1706–1716.

27 A. L. Goram and P. L. Richmond, Pegylated liposomal doxorubicin: Tolerability and toxicity, *Pharmacotherapy*, 2001, **21**, 751–763.

28 T. Mészáros, G. T. Kozma, T. Shimizu, K. Miyahara, K. Turjeman, T. Ishida, Y. Barenholz, R. Urbanics and J. Szebeni, Involvement of complement activation in the pulmonary vasoactivity of polystyrene nanoparticles in pigs: unique surface properties underlying alternative pathway activation and instant opsonization, *Int. J. Nanomed.*, 2018, **13**, 6345–6357.

29 S. Gómez-Ramírez, A. Shander, D. R. Spahn, M. Auerbach, G. M. Liumbruno, S. Vaglio and M. Muñoz, Prevention and management of acute reactions to intravenous iron in surgical patients, *J. Blood Transfus.*, 2018, **17**(2), 137–145.

30 P. Patel, A. Alghamdi, G. Shaw, C. Legge, M. Glover, D. Freeman, H. Hodgetts, E. Wilson, F. Howard, S. Staniland, A. J. Kennerley, D. Wood, R. Moorehead, C. Hadfield, O. Rominiyi, J. Griffin, S. J. Collis, S. Hyde, M. Crossley, M. Paley and M. Muthana, Development of a Personalised Device for Systemic Magnetic Drug Targeting to Brain Tumours, *Nanotheranostics*, 2023, **7**(1), 102–116.

31 Y. Meng, C. Shi, B. Hu, J. Gong, X. Zhong, X. Lin, X. Zhang, J. Liu, C. Liu and H. Xu, External magnetic field promotes homing of magnetized stem cells following subcutaneous injection, *BMC Cell Biol.*, 2017, **18**, 24.

32 S. A. Goraya, S. Ding, M. K. Arif, H. Kong and A. Masud, Effect of Circadian Rhythm Modulated Blood Flow on Nanoparticle based Targeted Drug Delivery in Virtual In Vivo Arterial Geometries, *Brain Multiphys.*, 2024, 100105.

33 M. P. Spencer and J. M. Reid, Quantitation of carotid stenosis with continuous-wave (C-W) Doppler ultrasound, *Stroke*, 1979, **10**(3), 326–330.

34 R. Ramirez-Carracedo, L. Tesoro, I. Hernandez, J. Diez-Mata, D. Piñeiro, M. Hernandez-Jimenez, J. L. Zamorano and C. Zaragoza, Targeting TLR4 with ApTOLL Improves Heart Function in Response to Coronary Ischemia Reperfusion in Pigs Undergoing Acute Myocardial Infarction, *Biomolecule*, 2020, **10**(8), 1167.

35 K. Sato, T. Wu, R. J. Laham, R. B. Johnson, P. Douglas, J. Li, F. W. Sellke, S. Bunting, M. Simons and M. J. Post, Efficacy of intracoronary or intravenous VEGF165 in a pig model of chronic myocardial ischemia, *J. Am. Coll. Cardiol.*, 2001, **37**(2), 616–623.

36 S. Pilote, C. Simard and B. Drolet, Fingolimod (Gilenya®) in multiple sclerosis: bradycardia, atrioventricular blocks, and mild effect on the QTc interval. Something to do with

the L-type calcium channel?, *Fundam. Clin. Pharmacol.*, 2017, **31**(4), 392–402.
37 N. L. Rumian, C. N. Brown, T. B. Hendry-Hofer, T. Rossetti, J. E. Orfila, J. E. Tullis, L. P. Dwoskin, O. R. Buonarati, J. E. Lisman, N. Quillinan, P. S. Herson, V. S. Bebarta and K. U. Bayer, Short-term CaMKII inhibition with tatCN19o does not erase pre-formed memory in mice and is neuroprotective in pigs, *J. Biol. Chem.*, 2023, **299**(5), 104693.